

Bound States in the Continuum in Zigzag Quantum Wire Enforced by a Finger Gate[†]

A. F. Sadreev^{a,*} and A. S. Pilipchuk^{a,b}

^a Kirensky Institute of Physics, Siberian Branch, Russian Academy of Sciences, Krasnoyarsk, 660036 Russia

^b Siberian Federal University, Krasnoyarsk, 660080 Russia

*e-mail: almas@tnp.krasn.ru

Received August 20, 2014; in final form, September 30, 2014

We consider electron transport in a zigzag quantum wire by the effect of finger gate potential. Using a non-Hermitian effective Hamiltonian, we calculate resonance positions and widths to show that the resonance widths are easily governed by the gate potential. In particular, the resonance width can be enforced to be equal to zero, which leads to an electron localization with the Fermi energy embedded in the propagation band of the wire, i.e., the bound state in the continuum (BSC). We show that, for positive values of the potential, a zigzag wire becomes a Fabry–Perot resonator to give rise to BSC too.

DOI: 10.1134/S0021364014210139

1. INTRODUCTION

In a single-electron approximation, ballistic electron transport in a directional quantum wire of width d is given by the wavefunctions

$$\psi_{\pm}(x, y) = \sqrt{\frac{1}{2\pi k_p}} \exp(\pm i k_p x) \phi_p(y), \quad (1)$$

where the Fermi energy of electron

$$E = \pi^2 p^2 + k_p^2, \quad k_p = \pi p/d, \quad p = 1, 2, 3, \dots \quad (2)$$

in terms of $E_0 = \frac{\hbar^2}{2m^*d^2}$, and

$$\phi_p(y) = \sqrt{\frac{2}{d}} \sin \frac{\pi p y}{d}. \quad (3)$$

How can an electron be localized in a clean wire? The first way is to bend the wire. That gives rise to a single bound state below the continuum of the wire for $E_F < \pi^2/d^2$ [1, 2]. This bound state is a result of the new length exceeding d because of bending. Olendski and Mikhailovska in pioneering work [3] demonstrated that, for a selected radius of bending, a localized bound state occurs with the energy above π^2/d^2 of the wire. However, experimental observation of such BSC faces difficulties in governing the bending radius.

There is a different way to capture a propagating electron using the Fano resonance [4]. Let us insert the in-channel scattering Anderson impurity in the directional wire which splits the transmission into two

paths: one path through the impurity and the second path which avoids the impurity. Interference of these paths can become fully destructive, resulting in complete reflection at some incident energy. Correspondingly, two identical impurities can realize a Fabry–Perot resonator (FPR). Such a FPR is capable of trapping an electron if the distance between impurities is fitted to an integer number of half De Broglie wavelengths. The FPR mechanism of electron localization was first considered by Shahbazyan and Raikh [5] for two impurities in the waveguide. Later, this mechanism was developed in temporally periodically driven one-dimensional wire [6] and quantum wire between quantum dots [7–10]. In [11], it was shown that the phenomenon of resonant capture in textured wires has the same origin as the bound states in the continuum (BSC) considered by von Neumann and Wigner [12] in a specially constructed spatially oscillating attractive potential. The localized BSC is the result of full destruction of resonant states [13–16]. Recently, the FPR mechanism of the BSC was considered in photonics [17, 18], which stimulated experimental observation of the phenomenon [19–24].

In the present work, we consider a zigzag quantum wire with a symmetrically positioned finger gate above the wire as shown in Fig. 1. We show that such a wire is capable of supporting two types of BSC. A positive finger gate potential can support the BSC by the FPR mechanism where bends of the wire can be considered as FPR “mirrors” at some electron Fermi energies, while the gate potential tunes effectively the distance between the “mirrors.” For a negative potential, the finger gate realizes the BSC because of cancellation of coupling of resonance inner states of the horizontal

[†]The article was translated by the authors.

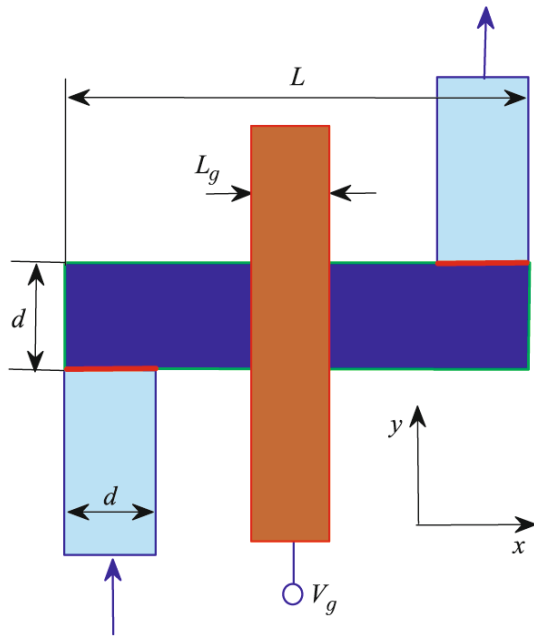


Fig. 1. (Color online) View of the zigzag wire with the finger gate shown in brown. Arrows show electron transport.

domain shown in deep blue in Fig. 1 with external propagating states (1) in vertical parts of the wires shown in light blue. That mechanism named “accidental” in [24–26] will be considered in the second section.

2. ELECTRON TRANSPORT THROUGH A ZIGZAG WIRE

Electron, microwave, and acoustic transmission in singly and doubly bent waveguides was considered in a number of works to demonstrate many features [27–30]. Among them, the transmission zeros and narrow resonance peaks shown in Fig. 2 are important for the present work. Each right-angle bend of the quantum wire gives a single transmission zero which is split in the doubly bent wire. It is easy to explain the resonant behavior of the conductance in the zigzag wire if we use the S-matrix description of electron transmission [31–35]

$$\hat{S} = \hat{W}[E^+ - \hat{H}_{\text{eff}}]^{-1} \hat{W}^+, \quad (4)$$

where

$$\hat{H}_{\text{eff}} = \hat{H}_B - i\pi \hat{W} \hat{W}^+ \quad (5)$$

is the non-Hermitian effective Hamiltonian. Here, \hat{H}_B is the Hamiltonian of the inner rectangular domain of the wire B colored in gray in Fig. 1, and the matrix \hat{W} is responsible for coupling of the inner states

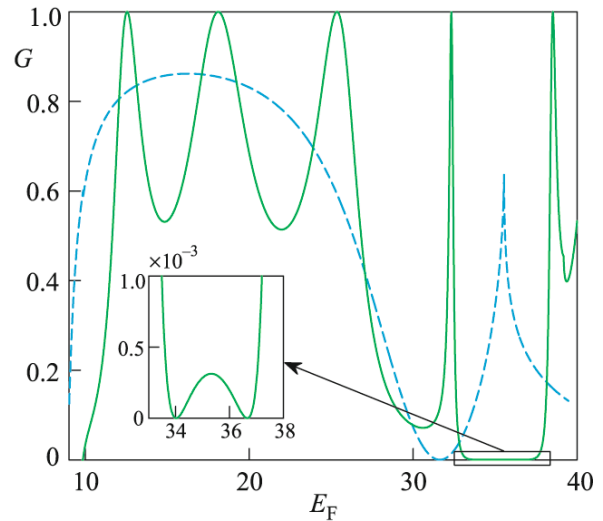


Fig. 2. (Color online) First channel conductance in the (solid line) zigzag wire and (dashed line) single bent wire.

$\psi_b(x, y)$ with the propagating waves (1) in waveguides. For the finger gate long compared to the wire’s width d , the inner states can be written as follows:

$$\psi_b(x, y) = \psi_m(x) \phi_n(y) = \sqrt{\frac{2}{d}} \sin\left(\frac{\pi n y}{d}\right) \psi_m(x), \quad (6)$$

where transversal eigenfunctions $\phi_n(y)$ coincide with the solutions in waveguides (1), $\psi_m(x)$ are the longitudinal eigenfunctions in a rectangular hard well of width L with implied potential $V_g(x)$ of the finger gate of width L_g . This potential is given by inverse trigonometric functions [36]. However, if the gate is spaced very close to the two-dimensional electron gas, the potential can be approximated by a rectangular shape with the height V_g and the width L_g [37]. In that case, the eigenfunctions $\phi_m(x)$ and eigenenergies $\epsilon(V_g)$ are given in textbook [38].

For the first channel, the transport matrix elements of the coupling matrix equal [34, 35, 39]

$$\begin{aligned} W_{m,n} &= \frac{1}{\sqrt{k_1}} \int_0^d dx \psi_1(x) \frac{\partial \psi_{m,n}(x, y=0, d)}{\partial y} \\ &= \frac{2}{\sqrt{k_1} d} \frac{\pi n}{d} \int_0^d dx \psi_1(x) \phi_m(x). \end{aligned} \quad (7)$$

The domain of integration is shown in Fig. 1 by bold red lines. The eigenfunctions of the inner part of the zigzag wire $\psi_m(x)$ are normalized to the length L . Therefore, the larger the ratio L/d , the smaller the overlapping integral given by Eq. (7) and, correspondingly, the narrower the resonances. The resonances are positioned at the eigenenergies $E_b = \epsilon_m + \pi^2 n^2 / d^2$.

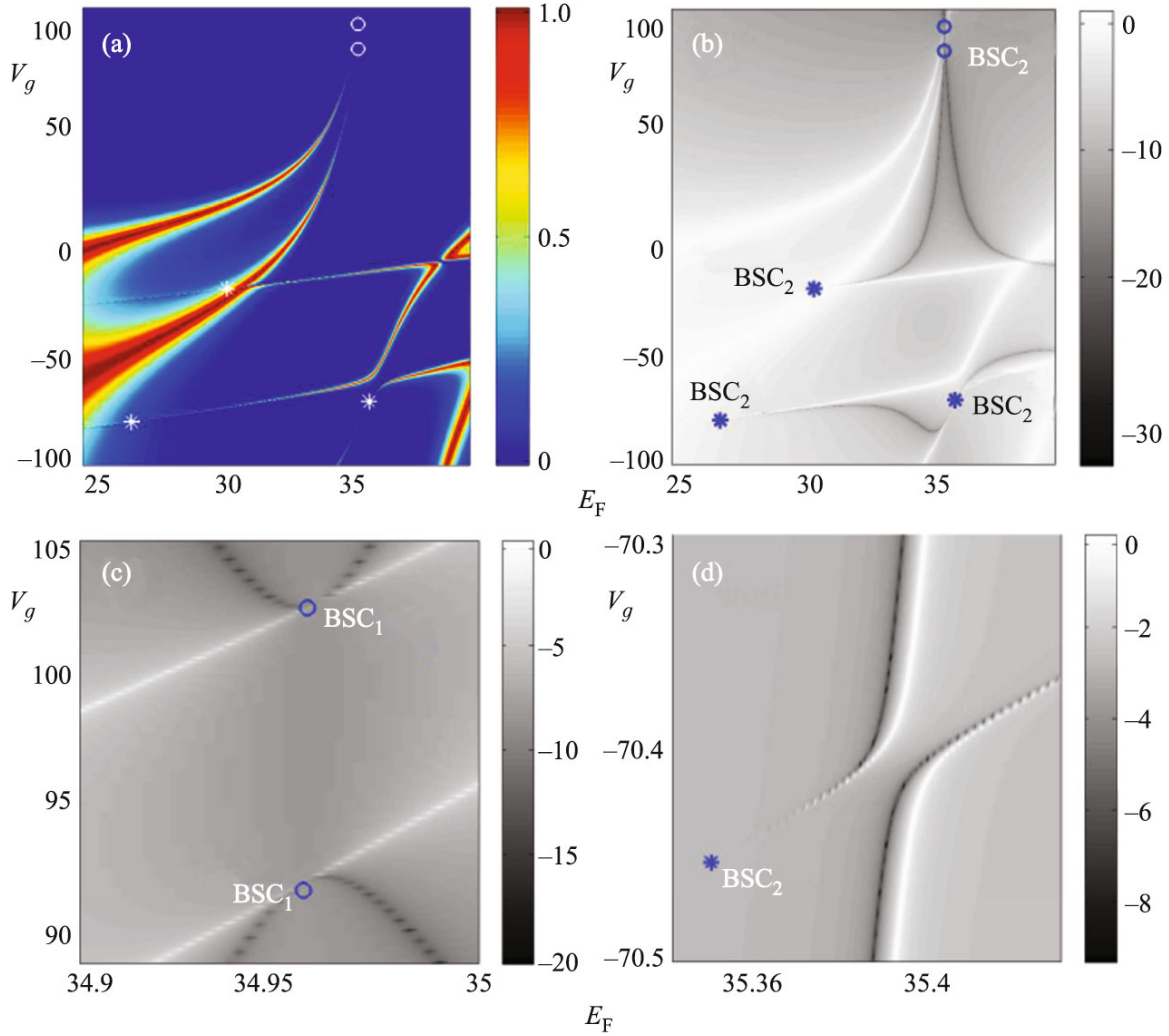


Fig. 3. (Color online) (a) Conductance of the zigzag wire with $L = 4d$ in the first channel $p = 1$ effected by finer gate potential with the width $L_g = d/2$. (b) The same on a log scale. The brightest part corresponds to maximal conductance and the darkest corresponds to zero conductance. Details of the conductance in the vicinity of BSC with $E = 34.95$, $V_g = 102.3$ (c) and $E = 35.34898$, $V_g = -70.4532$ (d).

Figure 3a shows the Landauer–Büttiker conductance [31] versus the Fermi energy and the finger gate potential which for the first channel transmission equals $G = |t|^2$ in terms of $2e^2/h$. The transmission amplitude t is given by the scattering matrix (4). In order to see features in the conductance, we presented also the conductance on a log scale in Fig. 3b.

The positions of the BSC in parametric space can be defined at those points where maximal unit transmission touches the zero one [15, 16, 19] marked in Fig. 3 by open circles and stars. At these points, a collapse of the Fano resonance occurs [40]. In order to demonstrate these peculiarities, we presented the fine structure of the conductance in the vicinity of the BSC in Figs. 3c and 3d. Rigorously, the BSC can be found from zeros of the resonance width $\Gamma_r = -2i\text{mag}(z(E_r))$ for variation of the potential V_g , where $E_r = \text{real}(z(E_r))$

[7, 8, 16, 33]. Calculation of poles of the scattering matrix is another way to find the BSC when a pole touches the real axis for variation of V_g [9, 10, 41, 42].

Evolution of real and imaginary parts of complex eigenvalues $z_\lambda(E)$ of the effective Hamiltonian (5) with variation of the finger gate potential V_g is shown in Fig. 4a. Only resonances embedded in the first channel continuum from $E = 25$ to $E = 38$ are presented. For positive V_g , the FPR mechanism for two BSC of the first type takes place with degenerate energies of 34.947 marked by red open circles. Figure 4b shows that these two BSC occur for different potentials. At $V_g < 0$, multiple BSC arise because of destructive interference of resonances (second type of BSC) marked in Fig. 4 by crosses. We show in Fig. 4b only a few BSC of the second type at $0 > V_g > -100$. For a wire 100 nm in

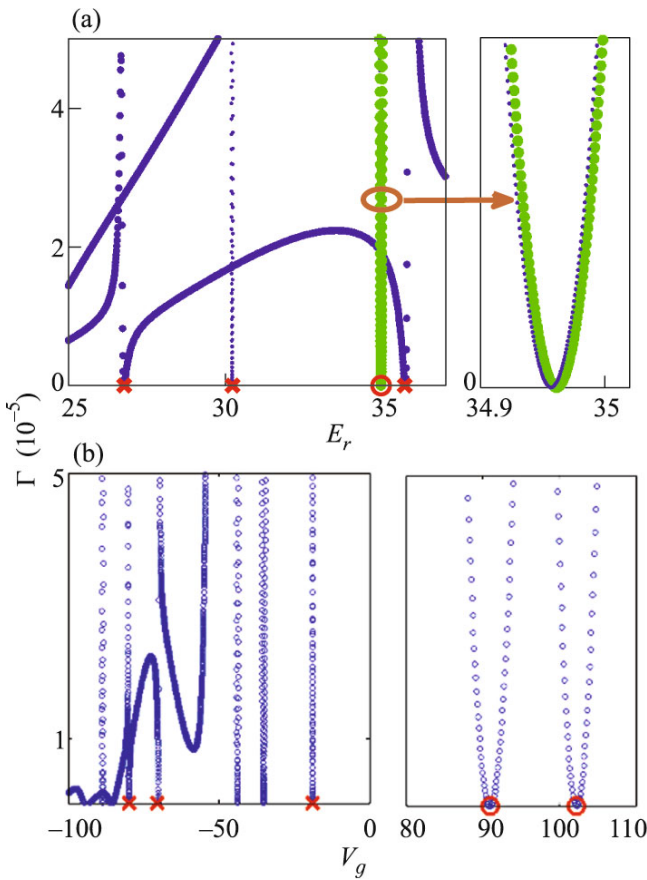


Fig. 4. (Color online) (a) Evolution of resonance positions and widths with V_g . (b) Resonant widths vs. V_g . Red crosses and open circles mark points where the resonance widths go to zero, which correspond to the BSC marked in Fig. 3 by stars and circles. The parameters of the wire are the same as in Fig. 3a.

width based on an In-doped GaAs interface, we have $E_0 \sim 0.1$ meV. Then, the dimensionless potential of 100 corresponds to 0.1 V.

The BSC wavefunctions presented in Fig. 5 clearly show a difference between the first and second types of BSC. One can see from this figure that the first two BSC are the result of the FPR mechanism with bends as “mirrors.” The second type is the result that the overlapping integrals $J_m = \int_0^L dx \psi_1(x) \phi_m(x)$ in Eq. (7) diminish as V_g decreases, as one can see from Fig. 6. In the inset in Fig. 6, we show how, in particular, integral J_6 tends to zero because the inner longitudinal eigenfunction $\phi_6(x)$ is subjected to deformation with growth of V_g .

3. CONCLUSIONS

We have considered electron transport in a zigzag quantum wire, where transport is maintained in the

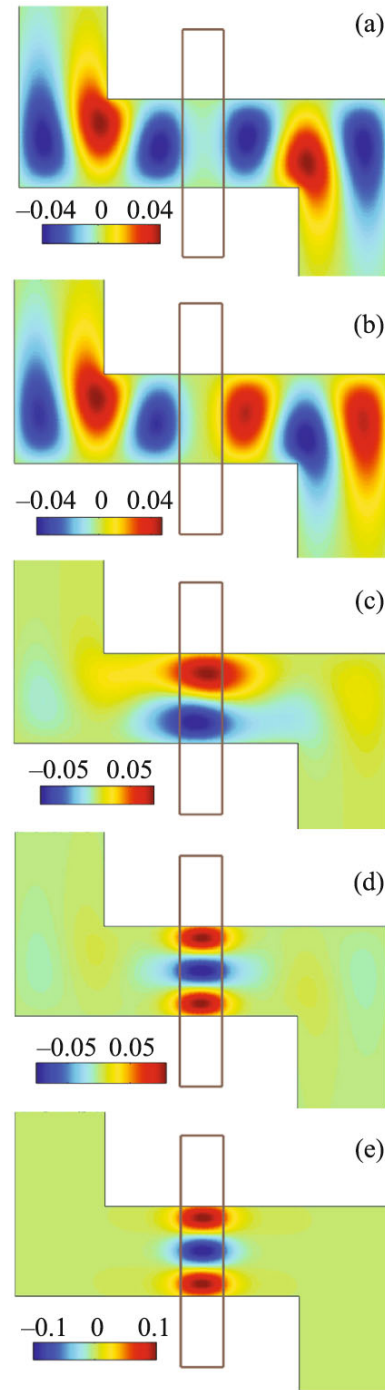


Fig. 5. (Color online) Patterns of BSC wavefunctions at the following parameters: (a) $E = 34.947$, $V_g = 90.95$; (b) $E = 34.947$, $V_g = 102.3$; (c) $E = 30.225$, $V_g = -18.908$; (d) $E = 35.34898$, $V_g = -70.4532$; and (e) $E = 26.779$, $V_g = -79.8495$. The finger gate is shown at the center.

first conduction channel. This problem has a long history [27–30]. The novelty of this work is in the prediction of the localization of a transport electron between bends owing to the forming of bound states with dis-

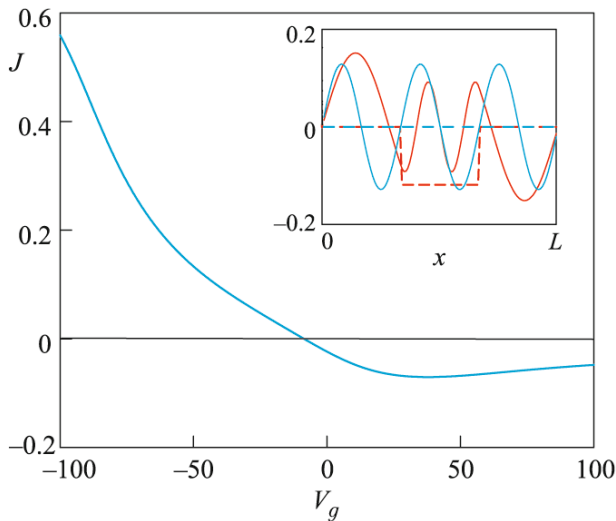


Fig. 6. (Color online) Overlapping integral of the inner eigenfunction $\phi_6(x)$ with the first channel propagating function $\psi_1 = \sqrt{\frac{2}{d}} \sin\left(\frac{\pi x}{d}\right)$ vs. V_g . The inset shows the inner function at the potential $V_g = 0$ (blue line) and $V_g = -100$. The red dashed line shows the potential profile along the x axis for $L = 3d$ and $L_g = d$.

crete energies in the continuum in the electron propagation band in the wire. Interest in bound states in the continuum has recently grown, particularly because of experimental visualization in photonics [19–24]. Bound states in the continuum shown in Fig. 5 clearly demonstrate that they are also not exotic in quantum wires. Furthermore, the proposed zigzag wire with a finger gate can be treated as a transistor that can control not only the transport properties, but also resonances until to vanishing of the resonance width (see Fig. 6). It is difficult to directly observe bound states in the continuum in microelectronic systems. However, they can be identified by features in the conductivity, where the collapse of Fano resonances occurs (see Fig. 3). The existence of such features was experimentally confirmed for the first time in [19] in a dielectric resonator placed in a microwave waveguide.

This work was supported by the Russian Foundation for Basic Research (project no. 14-12-00266).

REFERENCES

1. P. Exner and P. Šeba, *J. Math. Phys.* **30**, 2574 (1989).
2. Y. Avishai, D. Bessis, B. G. Giraud, and G. Mantica, *Phys. Rev. B* **44**, 8028 (1991).
3. O. Olendski and L. Mikhailovska, *Phys. Rev. B* **66**, 35331 (2002).
4. U. Fano, *Phys. Rev.* **124**, 1866 (1961).
5. T. V. Shahbazyan and M. E. Raikh, *Phys. Rev. B* **49**, 17123 (1994).
6. C. S. Kim and A. M. Satanin, *Phys. Rev. B* **58**, 15389 (1998).

7. I. Rotter and A. F. Sadreev, *Phys. Rev. E* **69**, 66201 (2004); *Phys. Rev. E* **71**, 046204 (2005).
8. A. F. Sadreev, E. N. Bulgakov, and I. Rotter, *JETP Lett.* **82**, 498 (2005).
9. G. Ordóñez, K. Na, and S. Kim, *Phys. Rev. A* **73**, 022113 (2006).
10. G. Cattapan and P. Lotti, *Eur. Phys. J. B* **60**, 51 (2007); *Eur. Phys. J. B* **66**, 517 (2008).
11. E. N. Bulgakov, K. N. Pichugin, A. F. Sadreev, and I. Rotter, *JETP Lett.* **84**, 430 (2006).
12. J. von Neumann and E. Wigner, *Phys. Z.* **30**, 465 (1929).
13. A. Z. Devdariani, V. N. Ostrovsky, and Yu. N. Sebyakin, *Sov. Phys. JETP* **44**, 477 (1976).
14. H. Friedrich and D. Wintgen, *Phys. Rev. A* **32**, 3231 (1985).
15. A. Volya and V. Zelevinsky, *Phys. Rev. C* **67**, 054322 (2003).
16. A. F. Sadreev, E. N. Bulgakov, and I. Rotter, *Phys. Rev. B* **73**, 235342 (2006).
17. D. C. Marinica, A. G. Borisov, and S. V. Shabanov, *Phys. Rev. Lett.* **100**, 183902 (2008).
18. E. N. Bulgakov and A. F. Sadreev, *Phys. Rev. B* **78**, 075105 (2008).
19. T. Lepetit, E. Akmansoy, J.-P. Ganne, and J.-M. Lourtios, *Phys. Rev. B* **82**, 195307 (2010).
20. Y. Plotnik, O. Peleg, F. Dreisow, M. Heinrich, S. Nolte, A. Szameit, and M. Segev, *Phys. Rev. Lett.* **107**, 183901 (2011).
21. G. Corrielli, G. della Valle, A. Crespi, R. Osellame, and S. Longhi, *Phys. Rev. Lett.* **111**, 220403 (2013).
22. S. Weimann, Y. Xu, R. Keil, A. E. Miroshnichenko, A. Tunnermann, S. Nolte, A. A. Sukhorukov, A. Szameit, and Yu. S. Kivshar, *Phys. Rev. Lett.* **111**, 240403 (2013).
23. Ch. W. Hsu, B. Zhen, J. Lee, S.-L. Chua, S. G. Johnson, J. D. Joannopoulos, and M. Soljacic, *Nature* **499**, 188 (2013).
24. B. Zhen, Ch. W. Hsu, L. Lu, A. D. Stone, and M. Soljacic, arXiv: 1408.0237v1 [physics.optics] (2014).
25. E. N. Bulgakov and A. F. Sadreev, *Phys. Rev. B* **83**, 235321 (2011).
26. Y. Yang, Ch. Peng, Y. Liang, Zh. Li, and S. Noda, *Phys. Rev. Lett.* **113**, 037401 (2014).
27. A. Weisshaar, J. Lary, S. M. Goodnick, and V. K. Tripathi, *Appl. Phys. Lett.* **55**, 2114 (1989).
28. J. C. Wu, M. N. Wybourne, W. Yindepol, A. Weisshaar, and S. M. Goodnick, *Appl. Phys. Lett.* **59**, 102 (1991).
29. Ch.-K. Wang, K.-F. Berggren, and Zh.-L. Ji, *J. Appl. Phys.* **77**, 2564 (1995).
30. J. P. Carini, J. T. Londergan, D. P. Murdock, D. Trinkle, and C. S. Yung, *Phys. Rev. B* **55**, 9842 (1997).
31. S. Datta, *Electronic Transport in Mesoscopic Systems* (Cambridge Univ. Press, Cambridge, UK, 1995).
32. H.-J. Stöckmann, *Quantum Chaos: An Introduction* (Cambridge Univ. Press, Cambridge, UK, 1999).

33. J. Okołowicz, M. Płoszajczak, and I. Rotter, *Phys. Rep.* **374**, 271 (2003).
34. A. F. Sadreev and I. Rotter, *J. Phys. A* **36**, 11413 (2003).
35. D. V. Savin, V. V. Sokolov, and H.-J. Sommers, *Phys. Rev. E* **67**, 026215 (2003).
36. J. H. Davies, I. A. Larkin, and E. V. Sukhorukov, *J. Appl. Phys.* **77**, 4504 (1995).
37. A. F. Sadreev and E. Ya. Sherman, *Phys. Rev. B* **88**, 115302 (2013).
38. S. Flügge, *Practical Quantum Mechanics*, Classics in Mathematics (Springer, Berlin, 1999; Mir, Moscow, 1974).
39. K. Pichugin, H. Schanz, and P. Seba, *Phys. Rev. E* **64**, 056227 (2001).
40. C. S. Kim, A. M. Satanin, Y. S. Joe, and R. M. Cosby, *Phys. Rev. B* **60**, 10962 (1999).
41. H. Nakamura, N. Hatano, S. Garmon, and T. Petrosky, *Phys. Rev. Lett.* **99**, 210404 (2007).
42. S. Hein, W. Koch, and L. Nannen, *J. Fluid Mech.* **692**, 257 (2012).